AGU PUBLICATIONS

JGR

Journal of Geophysical Research: Oceans

RESEARCH ARTICLE

10.1002/2016JC011906

Chromophoric and fluorescent dissolved organic matter in and above the oxygen minimum zone off Peru

A. N. Loginova[1], S. Thomsen[1], and A. Engel[1]

[1]GEOMAR Helmholtz Centre for Ocean Research Kiel, Kiel, Germany

Key Points:
- Two amino acid-like and three humic-like FDOM components were found in and above the oxygen minimum zone off the coast of Peru
- The distribution of CDOM and amino acid-like FDOM covaried with chl *a*, suggesting phytoplankton as their major source
- Presence of DOM microbial reworking and DOM release by anoxic sediment was illustrated by the distribution of humic-like FDOM

Supporting Information:
- Supporting Information S1

Correspondence to:
A. Engel,
aengel@geomar.de

Citation:
Loginova, A. N., S. Thomsen, and A. Engel (2016), Chromophoric and fluorescent dissolved organic matter in and above the oxygen minimum zone off Peru, *J. Geophys. Res. Oceans*, *121*, doi:10.1002/2016JC011906.

Received 20 APR 2016
Accepted 8 OCT 2016
Accepted article online 13 OCT 2016

Abstract As a result of nutrient upwelling, the Peruvian coastal system is one of the most productive regions in the ocean. Sluggish ventilation of intermediate waters, characteristic for the Eastern Tropical South Pacific (ETSP) and microbial degradation of a high organic matter load promotes deoxygenation at depth. Dissolved organic matter (DOM) plays a key role in microbial respiration and carbon cycling, but little is known on DOM distribution and cycling in the ETSP. DOM optical properties give important insights on DOM sources, structure and biogeochemical reactivity. Here, we present data and a conceptual view on distribution and cycling of chromophoric (CDOM) and fluorescent (FDOM) DOM in and above the oxygen minimum zone (OMZ) off Peru. Five fluorescent components were identified during PARAFAC analysis. Highest intensities of CDOM and of the amino acid-like fluorescent component (C3) occurred above the OMZ and coincided with maximum chl a concentrations, suggesting phytoplankton productivity as major source. High intensities of a marine humic-like fluorescent component (C1), observed in subsurface waters, indicated in situ microbial reworking of DOM. FDOM release from inner shelf sediment was determined by seawater analysis and continuous glider sensor measurement and included a humic-like component (C2) with a signature typical for terrestrially derived humic acids. Upwelling supplied humic-like substances to the euphotic zone. Photo-reactions were likely involved in the production of a humic-like fluorescent component (C5). Our data show that variable biological and physical processes need to be considered for understanding DOM cycling in a highly dynamic coastal upwelling system like the ETSP off Peru.

1. Introduction

The upwelling of cold and nutrient-rich water to the sea-surface stimulates high primary productivity in the Eastern Tropical South Pacific region (ETSP) [*Strub et al*., 1998; *Pennington et al*., 2006], leading to the production of labile and semilabile dissolved organic matter (DOM) in the upper water column [*Wood and Van Valen*, 1990]. Fresh DOM is used as substrate by heterotrophic communities, which, in turn, release less bioavailable semirefractory or even refractory DOM, thereby modifying the quantity and quality of the bulk DOM pool [*Azam et al*., 1983; *Ogawa et al*., 2001; *Jiao et al*., 2010]. Heterotrophic respiration of fresh organic matter and the associated oxygen consumption [*Kalvelage et al*., 2015] lead to a decrease in oxygen concentration with depth. In the ETSP, a pronounced thermal stratification of the upper water column [*Keeling et al*., 2010] and sluggish ventilation [*Stramma et al*., 2005] inhibit oxygen supply to intermediate waters [*Reid*, 1965]. As a result, the Peruvian upwelling system is characterized by an extensive Oxygen Minimum Zone (OMZ), with oxygen concentrations below 1 μmol O_2 kg^{-1} [*Revsbech et al*., 2009; *Kalvelage et al*., 2013; *Thomsen et al*., 2016].

Low concentrations of oxygen were shown to slow down microbial decomposition rates of major organic matter fractions, such as proteins, lipids and carbohydrates [*Harvey and Macko*, 1997]. Suboxic or anoxic conditions may also, eventually, lead to compositional changes in organic matter as the turnover time of individual compounds was shown to vary with oxygen concentrations [*Lee*, 1992].

Low oxygen conditions together with high organic matter supply force microbial communities to seek new sources of energy for redox processes [e.g., *Kirchman*, 2012], therefore activating nitrogen (N)-loss processes, such as denitrification and anaerobic ammonia oxidation (anammox) [*Strous et al*., 2006; *Kartal et al*., 2007; *Jayakumar et al*., 2009; *Jetten et al*., 2009; *Chang et al*., 2014]. Those processes result in a lack of bioavailable N with respect to the classical Redfield ratio [*Redfield*, 1958]. The changes in bioavailable N concentrations may not only affect productivity above OMZs, but also influence the quantity and quality of DOM

[*Kramer and Herndl*, 2004; *Stedmon and Markager*, 2005; *Biers et al*., 2007; *Conan et al*., 2007; *Engel et al*., 2015]. Thus, a decrease in bioavailable inorganic N at constant inorganic phosphorus (P) concentrations may lead to reduction in an accumulation of dissolved organic carbon (DOC) [*Conan et al*., 2007; *Loginova et al*., 2015] and to substantial decrease in production of the chromophoric (CDOM) and fluorescent (FDOM) DOM fractions [*Stedmon and Markager*, 2005; *Biers et al*., 2007; *Loginova et al*., 2015]. Furthermore, heterotrophic uptake of DOM may be accompanied by consumption of inorganic N in form of nitrate, and therefore, presence of inorganic N was assumed to be a regulator of microbial DOM availability [*Kirchman et al*., 1991].

CDOM and FDOM represent optically active DOM fractions and have often been used for estimation of DOM quantity and quality [*Stedmon and Nelson*, 2015]. The DOM fraction referred to as CDOM represents the light absorbing molecules [*Coble*, 2007], while FDOM is a CDOM fraction, which is able to fluoresce [*Stedmon and Álvarez-Salgado*, 2011].

CDOM embodies a mixture of organic compounds of different content and complexity, and therefore it absorbs light in a wide spectral range (230–750 nm) with no discernible peaks [*Del Vecchio and Blough*, 2004]. CDOM abundance is commonly expressed as absorption coefficient at chosen wavelength (e.g., 325, 355, 375 nm) [*Stedmon and Markager*, 2001; *Fichot and Benner*, 2012; *Nelson and Siegel*, 2013]. Spectral characteristics of CDOM, such as spectral slopes (S) of CDOM light absorption and the ratio of specific spectral slopes (S_R) are used as indicators for changes in CDOM molecular weight and photo reactivity [*Helms et al*., 2008, *Zhang et al*., 2009]. S was shown to decrease with increasing DOM molecular weight [*De Haan and De Boer*, 1987; *Helms et al*., 2008; *Zhang et al*., 2009], and S_R increases as CDOM becomes involved in photoreactions and decreases as CDOM undergoes microbial reworking [*Helms et al*., 2008]. In other means, an increase in S_R indicates that CDOM is largely degraded and is dominated by DOM of lower molecular weight.

FDOM measurements may be used to estimate DOM bulk characteristics, and also to discriminate between DOM pools [*Zsolnay et al*.; 1999; *Zsolnay*, 2003; *Coble*, 2007; *Mopper et al*., 2007; *Stedmon and Bro*, 2008; *Huguet et al*., 2009; *Yamashita et al*., 2010]. Thus, fluorescence indexes, derived from Excitation and Emission (Ex/Em) spectra, may be used as proxies for DOM properties. The humification index (HIX) is often calculated as an estimate of the degree of DOM maturation [*Zsolnay et al*., 1999; *Zsolnay*, 2003] and the biological/autochtonous index (BIX) is used to assess biological modification of DOM [*Huguet et al*., 2009]. The Ex/Em spectra of FDOM are used also to identify different DOM pools [*Coble*, 2007; *Mopper et al*., 2007; *Stedmon and Bro*, 2008; *Yamashita et al*., 2010]. Compounds that are excited and emit in the UV spectral range commonly correspond to labile proteinaceous DOM, and are referred to as amino acid-like (tyrosine- and tryptophan-like) FDOM [*Coble*, 1996]. Substances that are excited in the UV spectral range, but emit in the visible spectral range were identified as fulvic- and humic-like FDOM components [*Coble*, 1996; *Guéguen and Kowalczuk*, 2013] and have been related to semirefractory or refractory DOM [*Coble*, 1996].

Optically active DOM may be used for carbon assessment in aquatic systems, where DOM cycling is controlled by conservative mixing. Thus, CDOM absorption has been used to estimate DOC concentrations in field studies [*Fichot and Benner*, 2012; *Rochelle-Newall et al*., 2014]. In remote sensing techniques, light attenuation is used by satellites to derive CDOM signal, and, by assuming a direct relationship between CDOM absorption and DOC concentrations, the distribution of DOC in surface waters [*Del Castillo*, 2007]. Furthermore, the fluorescence signal of CDOM, measured by in situ fluorometers (e.g., WETStar, TriOS), revealed a potential for strong relationship to DOC in areas, where the input of terrestrial DOM is considerable [*Belzile et al*., 2006; *Saraceno et al*., 2009; *Kowalczuk et al*., 2010]. In the open ocean, however, CDOM absorption does not reveal a simple linear relationship to DOC [*Nelson and Siegel*, 2013], as the relationship is driven by more complex processes than conservative mixing. Some attempts for developing nonlinear relationship between carbon specific CDOM absorption and spectral slope have been done in coastal regions [*Fichot and Benner*, 2012], as well as in mesocosms simulating open ocean conditions [*Loginova et al*., 2015]. Those relationships, however, still need to be tested in different ocean regions.

Even though the ETSP was recognized to be an important source of organic matter and its OMZ may be potentially important for cycling of carbon and other elements, still little is known about the distribution and cycling of DOM in this region. As CDOM and FDOM may serve as proxies for the quantity and quality of DOM, we examined the distribution and cycling of optically active DOM in and above the OMZ off the coast of Peru during M93 research cruise onboard the RV METEOR that took place from 7 February to 9 March 2013.

We used measurements of CDOM absorption and FDOM excitation emission matrix spectroscopy (EEM) followed by PARAFAC analysis as well as measurements by a glider-mounted CDOM fluorometer. The CDOM absorption and FDOM measurements were compared to salinity, as well as to oxygen, DOC, dissolved organic nitrogen (DON) and nutrients concentrations in order to identify processes influencing DOM cycling in and above the OMZ off the coast of Peru.

2. Materials and Methods

2.1. Study Area

This study was conducted as a part of a multiplatform observational experiment in the Peruvian upwelling system between 12°S and 14°S and 76°W and 79°W (Figure 1). The M93 cruise onboard R/V METEOR took place from 7 February to 9 March 2013. During the measurements, the study area was affected by moderate southeasterly winds (1–9 m/s) [*Thomsen et al*., 2016], resulting in nutrient upwelling. These conditions are, likely, representative for austral summer season conditions as Oceanic Niño Index revealed very low values for 2013 (−0.5–0) (according to *Null* [2016]). In summer season, ETSP is characterized by high water column stratification, and therefore, the productive mixed layer is limited to 5–70 m depth [*Echevin et al*., 2008; *Franz et al*., 2012]. As a result of upwelling, the oxycline is typically found between 5 m and 70 m depth as well. Therefore, low oxygen (<1 μmol kg^{-1}) [*Revsbech et al*., 2009; *Kalvelage et al*., 2013] and also high concentrations of inorganic nutrients (∼30 μmol L^{-1} [NO_3^-], ∼3 μmol L^{-1} [PO_4^{3-}]) [*Franz et al*., 2012] can be found just below the mixed layer.

2.2. Discrete Water Sampling and Analysis

Discrete water sampling was accomplished at 22 stations along two parallel transects that were located between 12°13′ and 12°43′ S and 77°10′ and 77°49′ W (Figure 1). Seawater was sampled with a GO rosette equipped with 24 × 10 L bottles at 3 to 8 sampling depths from 2 to 70 m at the most nearshore stations (∼10 km offshore) and from 2 to 200 m at stations offshore (∼90 km offshore).

The rosette was equipped with a conductivity, temperature and depth recorder (CTD; Sea-Bird SBE 9-plus, Sea-Bird Electronics Inc., USA), oxygen optode (Sea-Bird SBE 9-plus, Sea-Bird Electronics Inc., USA), and a

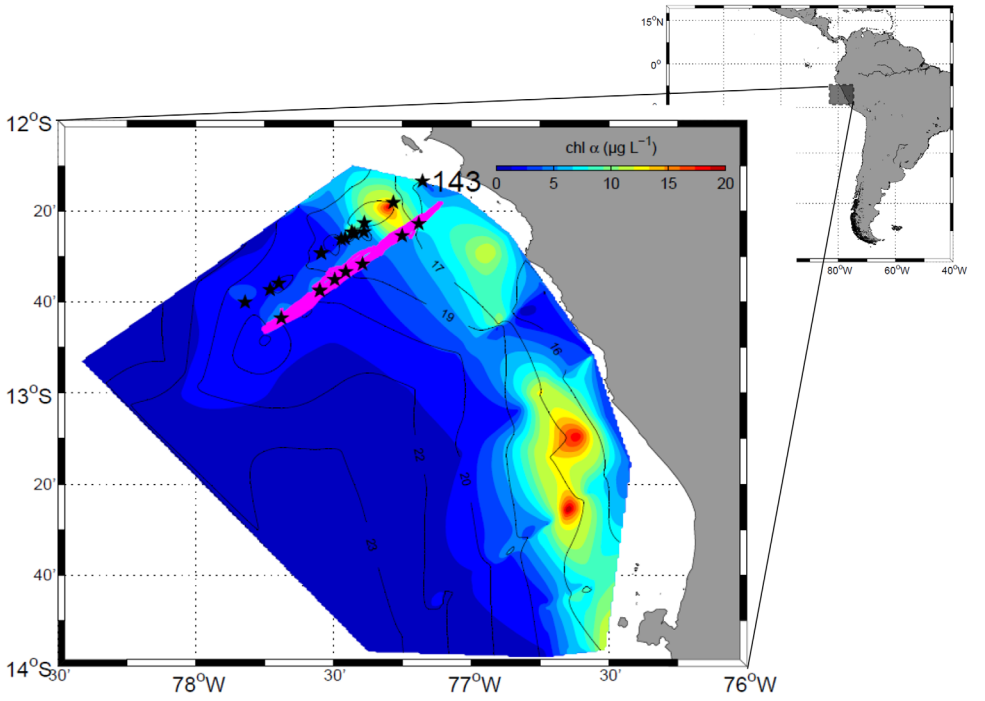

Figure 1. The study area of the M93 RV METEOR cruise. The color shaded areas represent the distribution of chl *a* (μg L^{-1}) and the isolines depict the temperature distribution at 5 m depth. Sampling stations along two investigated transects, which were combined into one for illustrating of vertical distribution of different parameters, are indicated by black stars. The glider trajectory is marked with magenta color.

WETStar chl *a* fluorometer (WET Labs, USA). The conductivity probe was calibrated with discrete seawater samples measured with Guildline Autosal 8 model 8400B salinometer. The oxygen optode was calibrated by a combination of Winkler titration [*Winkler*, 1888; *Grasshoff et al*., 1983] and STOX sensor measurements [*Revsbech et al*., 2009]. Salinity and oxygen had detection limits (DL) of 0.002 g kg^{-1} and ~1 μmol kg^{-1}, respectively. More details on the salinity and oxygen calibrations can be found in *Thomsen et al*. [2016].

The original calibration of in situ chl *a* fluorometer, provided by the sensor manufacturer (WET Labs, USA), was used throughout the cruise, resulting in chl *a* concentrations expressed in μg L^{-1}. Water samples from night-time CTD casts were filtered and the extracted chl *a* was determined in the laboratory [*J. Meyer*, pers. com.]. The resulting 142 concentration values were compared to the chl *a* readings from the chl *a* fluorometer at the time of the bottle closing. A linear regression analysis showed no significant offset and a slope of 1.04 ± 0.03 [*G. Krahmann*, pers. com.]. As the determined slope did not differ significantly from unity, we refrained from applying the small calibration factor and used the data as given by the fluorometer.

Duplicate samples for inorganic nutrients––[NO_3^-], [NO_2^-], [NH_4^+], [PO_4^{3-}]––were collected into sterile 50 mL falcon tubes and analyzed after *Grasshoff et al*. [1983], as described in *Thomsen et al*. [2016]. DL for determination of [NO_3^-], [NO_2^-], [NH_4^+], [PO_4^{3-}] were 0.05, 0.01, 0.5, and 0.05 μmol L^{-1}, respectively.

DOC/DON duplicate samples (20 mL) were filtered through combusted GF/F filters (5 h, 450°C) and collected in combusted glass ampoules (8 h, 450°C). Samples were acidified with 80 μL of 85% phosphoric acid, flame sealed and stored at 4°C in the dark until analysis.

DOC samples were analyzed by applying the high-temperature catalytic oxidation method (TOC -VCSH, Shimadzu) modified from *Sugimura and Suzuki* [1988], with DL of 1 μmol L^{-1}. The calibration and measurements routine is described in more detail in *Loginova et al*. [2015]. Total dissolved nitrogen (TDN) was determined simultaneously to DOC with DL of 2 μmol L^{-1} using the TNM-1 detector of a Shimadzu analyzer [*Dickson et al*., 2007]. The instrument was calibrated every 8–10 days by analyzing 5 standard solutions of 0, 100, 250, 500, and 800 μg N L^{-1}, prepared from a potassium nitrate Suprapur® (Merk 105065) solution. DON concentrations were calculated by subtracting sum of NO_3^-, NO_2^-, and NH_4^+ concentrations from concentration of TDN.

For FDOM, 15mL samples were collected into combusted (450°C, 8 h) amber-glass vials after filtering through 0.2 μm polyethersulfone syringe filters (CHROMAPHIL® Xtra PES-45/25) and then stored frozen (−20°C). Samples were brought to room temperature before analyses.

Spencer et al. [2007] and *Thieme et al*. [2016] reported that fluorescence properties of DOM may change at temperatures below 0°C. The change in DOM properties could be caused by bacteria cell rapture during freezing and/or by flocculation during brine water formation of highly concentrated DOM samples, characteristic for rivers and grassland or forest soils, which were studied in *Spencer et al*. [2007] and *Thieme et al*. [2016], respectively. On the other hand, in studies, where samples were prefiltered (0.2–0.45μm) and FDOM concentrations were relatively low, sample-freezing was not found to bias measurements or to add inter-replicate variability [*Yamashita et al*., 2010; *Murphy et al*., 2013a]. In our study, the freezing of our samples could not be avoided due to logistical reasons. Since we got rid of most of the bacterial cells during 0.2μm filtration, and collected DOM samples were relatively diluted, we believe that freezing effects on FDOM during our studies were of minor importance.

For the determination of FDOM, 3D-EEM fluorescence spectroscopy was performed using a Cary Eclipse Fluorescence Spectrophotometer (Agilent Technologies) equipped with a xenon flash lamp. The fluorescence spectra for samples were measured in a 4-optical window 1 cm Quartz SUPRASIL® precision cell (Hellma®Analytics). Blank-3D fluorescence spectra and Water Raman scans were performed daily using an Ultra-Pure Water Standard sealed cuvette (3/Q/10/WATER; Starna Scientific Ltd). The experimental wavelength range for sample and ultrapure water scans was 230 to 455 nm in 5 nm intervals on excitation and 290 to 700 nm in 2 nm intervals on emission. The Ex/Em scans were later cut to intervals from 260 to 455 nm for excitation and from 300 to 500 nm for emission in order to reduce potential noise during PARAFAC analysis. Water Raman scans were recorded from 285 to 450 nm at 1 nm intervals for emission at the 275 nm excitation wavelength [*Murphy et al*., 2013b]. All fluorescence measurements were conducted at 19°C, controlled by Cary Single Cell Peltier Accessory (VARIAN), PMT 900V, 0.2 s integration times and 5 nm slit width on excitation and emission monochromators.

For CDOM, 35 mL samples were collected into combusted (450°C, 8 h) amber-glass vials after filtering through 0.2 μm polyethersulfone syringe filters (CHROMAPHIL® Xtra PES-45/25, MACHEREY-NAGEL GmbH &

Co.KG) and stored at 4°C in the dark pending analyses (1–14 days). Samples were brought to room temperature (~19°C) before analyses. The CDOM absorbance was measured with Shimadzu® 1800 UV-VIS double-beam spectrophotometer using 5 cm Quartz SUPRASIL® precision cell (Hellma®Analytics) at 1 nm wavelengths intervals from 230 to 750 nm against MilliQ water as a reference. CDOM spectra from 275 to 400 nm were used for recalculation to absorption coefficients (see section 2.4).

2.3. Glider Measurements

A CTD cell and an ECO Triplet FLBBCD-SLK Puck sensor (WETStar CDOM fluorometer) configured for measurements at Excitation/Emission (Ex/Em) 370/460 nm (WETLabs, USA) mounted on Slocum glider (Teledyne 126 Webb Research) were used for high-resolution measurement of salinity and CDOM fluorescence, respectively, along the transect that is shown in Figure 1.

The Ex/Em=370/460 nm is commonly used for CDOM sensor configuration, as fluorescence maximum at those wavelengths represents a signal of quinine sulfate (QS), which is considered to be a reference substance for aquatic humic acids. That signal also was shown to have great potential for correlation to DOC at aquatic sites [*Saraceno et al*., 2009; *Conmy et al*., 2014]. Therefore, measurements by CDOM fluorometer mounted on a Slocum glider gave an opportunity to receive data of high lateral resolution (~200 m) of fluorescence of humic-like substances in the area off coast of Peru and to compare those with fluorescence analyses of discrete water samples.

The Slocum glider (Teledyne 126 Webb Research) was deployed on 7 January 2013, as part of a multiglider observational experiment and remained in the water autonomously. The glider continuously measured CDOM fluorescence moving in upper 200 m of the water column along the transect, indicated on Figure 1, until it was recovered on 1 March 2013. During the full measurement time period it provided 3099 profiles [*Thomsen et al*., 2016]. Eight glider profiles were later used for comparison with discrete water samples and 955 glider profiles were used for graphical representation of spatial variability of optically active DOM.

2.4. Data Evaluation

Data from both transects were merged into one plot for each of investigated parameters, as both transects were located in the vicinity to each other (~13 km). Data for each parameter were plotted against distance from the coast, calculated separately for each transect before merging. The data were interpolated between data points by "TriScatterInterp" function (*MatLab*, 2012b) (The MathWorks Inc.) for graphical representation. As no extrapolation was done, it resulted in white areas for investigated parameters at depths, where no samples were taken.

CDOM absorbance spectra were converted to absorption coefficients according to *Bricaud et al*. [1981]:

$$a_{CDOM}(\lambda) = \frac{2.303A(\lambda)}{L}; \quad (1)$$

where $a_{CDOM}(\lambda)$ is the absorption coefficient at wavelength λ (m^{-1}), $A(\lambda)$ is the absorbance value at same wavelength and L is the effective optical path length (m).

Open ocean waters show only very low absorbance at wavelengths of 400–600 nm. Therefore, absorption at 325 nm (a_{CDOM} (325)) was used as a proxy for open ocean CDOM concentrations [*Nelson and Siegel*, 2013].

Spectral slopes for the intervals 275–295 nm ($S_{275-295}$) and 350–400 nm ($S_{350-400}$) were calculated after *Helms et al*. [2008] using log-transform linear regression. The CDOM alteration indicator, slope ratio (S_R), was calculated after *Helms et al*. [2008] as the ratio of $S_{275-295}$ and $S_{350-400}$.

The 3D fluorescence spectra were corrected for spectral bias, background signals and inner filter effects after *Murphy et al*. [2013b]. Each EEM was normalized to the area of the ultra-pure water Raman peaks, measured at the same day. EEMs were combined into four-dimensional data array and analyzed by PARAFAC [*Stedmon and Bro*, 2008]. The 5-component least square model was developed out of 10 repeat runs; the model validation was obtained by split-half analysis, using "drEEM toolbox for MATLAB" after *Murphy et al*. [2013b]. The 5-component model could be validated only for samples that were taken from upper 50 m of the water column, below 50 m depth the fluorescence of the fifth component was low (comparable to instrument noise), and therefore validation of samples that were taken below 50 m depth of the water column could not be accomplished successfully.

The humification index (HIX) was calculated as

$$HIX = \frac{H}{L}; \quad (2)$$

where H is an area below intensity peak between 434 and 480 nm on emission at 255 nm on excitation and L is below intensity peak between 300 and 346 nm on emission at 255 nm on excitation [*Zsolnay et al.*, 1999]. Both areas were calculated as an area of trapezoid under the curve [*MatLab*, 2012b] (The MathWorks Inc.).

The biological/allochtonous index (BIX) was calculated as:

$$BIX = \frac{I_{Em=380}}{I_{Em=430}}; \quad (3)$$

where, $I_{Em=380}$ is the fluorescence intensity at 380 nm exited at 310 nm, and $I_{Em=430}$ is the fluorescence intensity at 380 nm exited at 310 nm [*Huguet et al.*, 2009].

For comparison of CDOM fluorescence obtained by the glider sensor with FDOM data obtained by EEM at discrete locations, the glider data were extracted in such way that temporal and spatial gaps between sensor data and water samples were minimal. Then, the data from water samples and extracted glider CDOM values were tested for covariance by linear regression analysis.

3. Results and Discussion

3.1. Oceanographic Settings on the Transect

Along transects, temperature of the upper mixed layer ranged from approximately 16°C at the most nearshore stations to >20°C offshore. Below 5 – 60 m, temperatures ranged from 12 to 14°C (Figure 2). Highest oxygen concentrations (up to 250 μmol kg^{-1}) occurred near the surface. Below 5 - 50m, oxygen concentrations decreased abruptly, reaching < 1 μmol kg^{-1} (Figure 2).

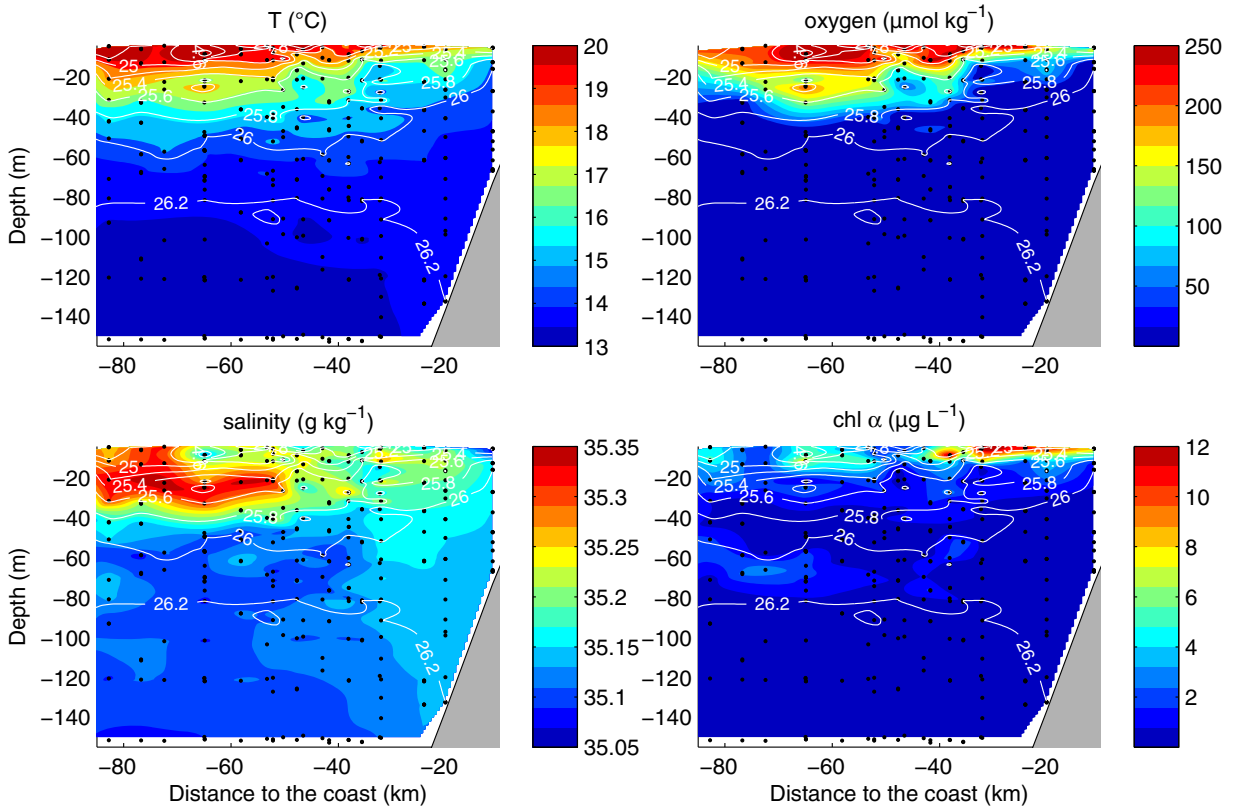

Figure 2. Vertical distributions of temperature, salinity, dissolved oxygen and chl *a* along the combined transect. The coastal slope is shaded in gray. Black dots represent the locations of taken samples. White isolines depict potential density distribution.

Highest salinities of 35.35 g kg^{-1} were found near the surface. A high salinity plume (>35.20 g kg^{-1}) centered at 20 m (Figure 2) and was referred to as Subtropical Surface Water (STSW) [*Wyrtki*, 1967; *Fiedler and Talley*, 2006; *Silva et al*., 2009; *Thomsen et al*., 2016]. In the water column that was not influenced by STSW, relatively high salinities could be found near the surface (35.15 – 35.20 g kg^{-1}). At depth, observed salinities ranged between 35.05 and 35.15 g kg^{-1}. Two other water masses, Equatorial Subsurface Water (ESSW) [*Gunther*, 1936; *Silva et al*., 2009; *Thomsen et al*., 2016] and Eastern South Pacific Intermediate Water (ESPIW) [*Schneider et al*., 2003; *Silva et al*., 2009; *Thomsen et al*., 2016] might have had an effect on the salinity distribution in deeper waters. Furthermore, the water mass distribution was strongly influenced by mesoscale along-isopycnal stirring due to the formation of an eddy in the study area [*Thomsen et al*., 2016].

Highest chl *a* concentrations (4–20 μg L^{-1}) were observed within upper 5 to 20 m. A second chl *a* maximum (1–2 μg L^{-1}) was observed at offshore stations at approximately 60–80 m (Figure 2). Surface water with high concentrations of chl *a* and salinities lower than 35.15 g kg^{-1} was defined as "surface salinity minimum" (SSMW) water (supporting information Figure S1).

During the study, a shallow nutricline was observed at ~5 m at the most nearshore stations and between 30 and 40 m offshore (Figure 3). Nitrate and phosphate were lower in surface waters (below DL-1.00 μmol L^{-1} and 0.50–1.00 μmol L^{-1}, respectively) increasing to maximum values of ~25.00 and 2.00 μmol L^{-1}, respectively, at depth. Maximum nitrite concentrations of 6.0 μmol L^{-1} were observed below 80 m depth, where nitrate concentrations slightly decreased to ~ 20.00 μmol L^{-1}.

On the shelf (St. 143, Figure 1 and supporting information Table S1) maximum values of phosphate (~3 μmol L^{-1}) and ammonia (up to 4 μmol L^{-1}) could be indicated near the sediment (20 - 60 m depth), while the concentrations of nitrate and nitrite at those depth were below DL (<0.05 μmol L^{-1}, Figure 3 and supporting information Figure S1). This low in inorganic nitrogen (N) and high in inorganic phosphorus (P) water was referred as "low nitrogen water" (LNW) during this study (supporting information Figure S1).

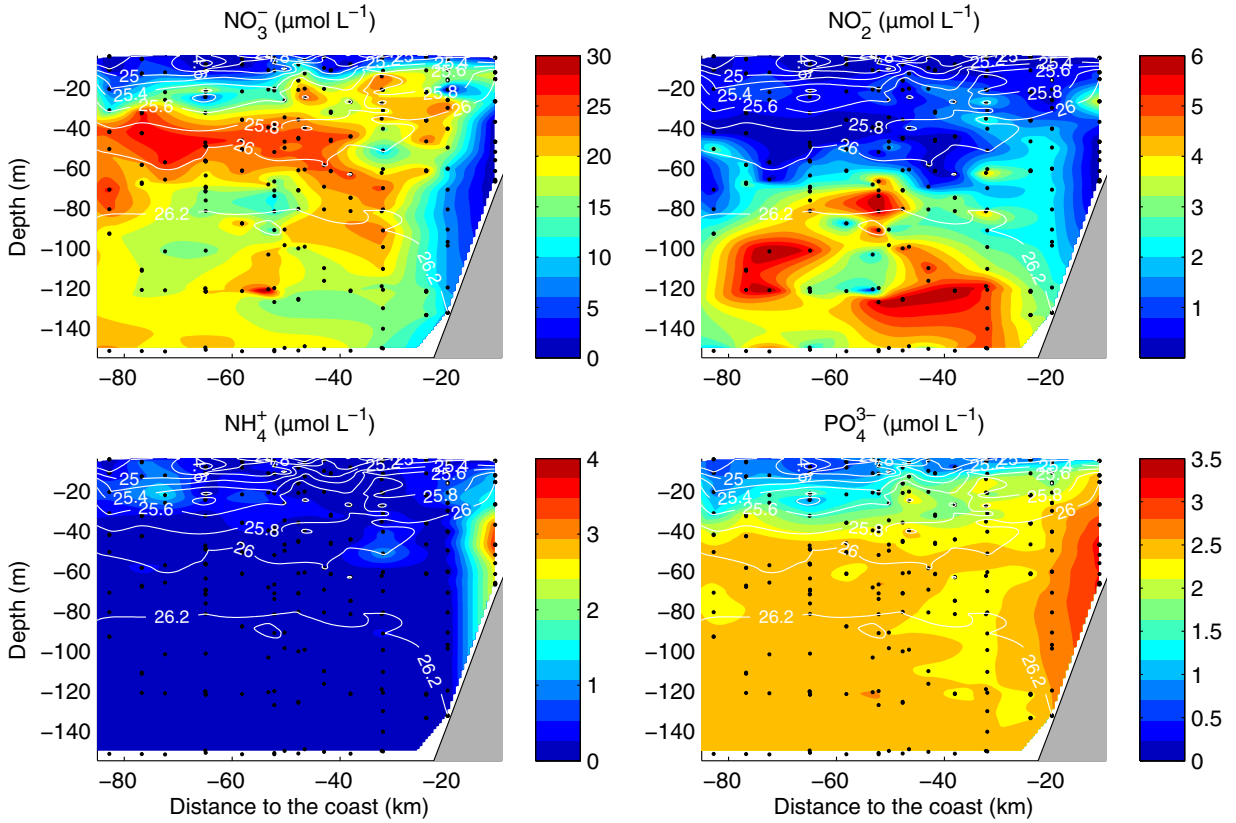

Figure 3. Vertical distributions of dissolved nitrate, nitrite, ammonia and phosphate along the combined transect. The coastal slope is shaded in gray. Black dots represent the locations of taken samples. White isolines represent potential density distribution.

Part of the investigated transect, that did not include STSW, LNW or SSMW was referred as "high nitrogen water" (HNW) during this study (supporting information Figure S1), as it contained the highest concentrations of nitrate (~20 μmol L^{-1} on average).

3.2. Characteristics of DOM

DOC concentrations ranged from less than 50 μmol L^{-1} in HNW to more than 120 μmol L^{-1} in SSMW. In STSW, DOC concentrations were 70–80 μmol L^{-1}. At the vicinity to sediments (LNW) DOC was accumulated up to 80–100 μmol L^{-1} (Figure 4). The range of DOC concentrations, obtained during the M93 research cruise, is in an agreement with previous studies in ETSP, as reported previously values varied from 40 to 300 μmol L^{-1} [*Romankevich and Ljutsarev*, 1990; *Franz et al*., 2012; *Engel and Galgani*, 2015].

Lowest DON concentrations were observed (<3 μmol L^{-1}) in HNW, while in LNW, DON concentrations up to ~4 μmol L^{-1} were determined (Figure 4). Both, SSMW and STSW, contained DON concentrations of about 4–6 μmol L^{-1}. Those concentrations are slightly higher than concentrations reported previously for the upper 50 m of the water column of eastern subtropical South Pacific (4.3 ± 0.5 μmol L^{-1}) [*Letscher et al*., 2013]; a slightly higher DON accumulation may be reasoned by higher productivity that is characteristic to upwelling regimes compared to central ocean basins.

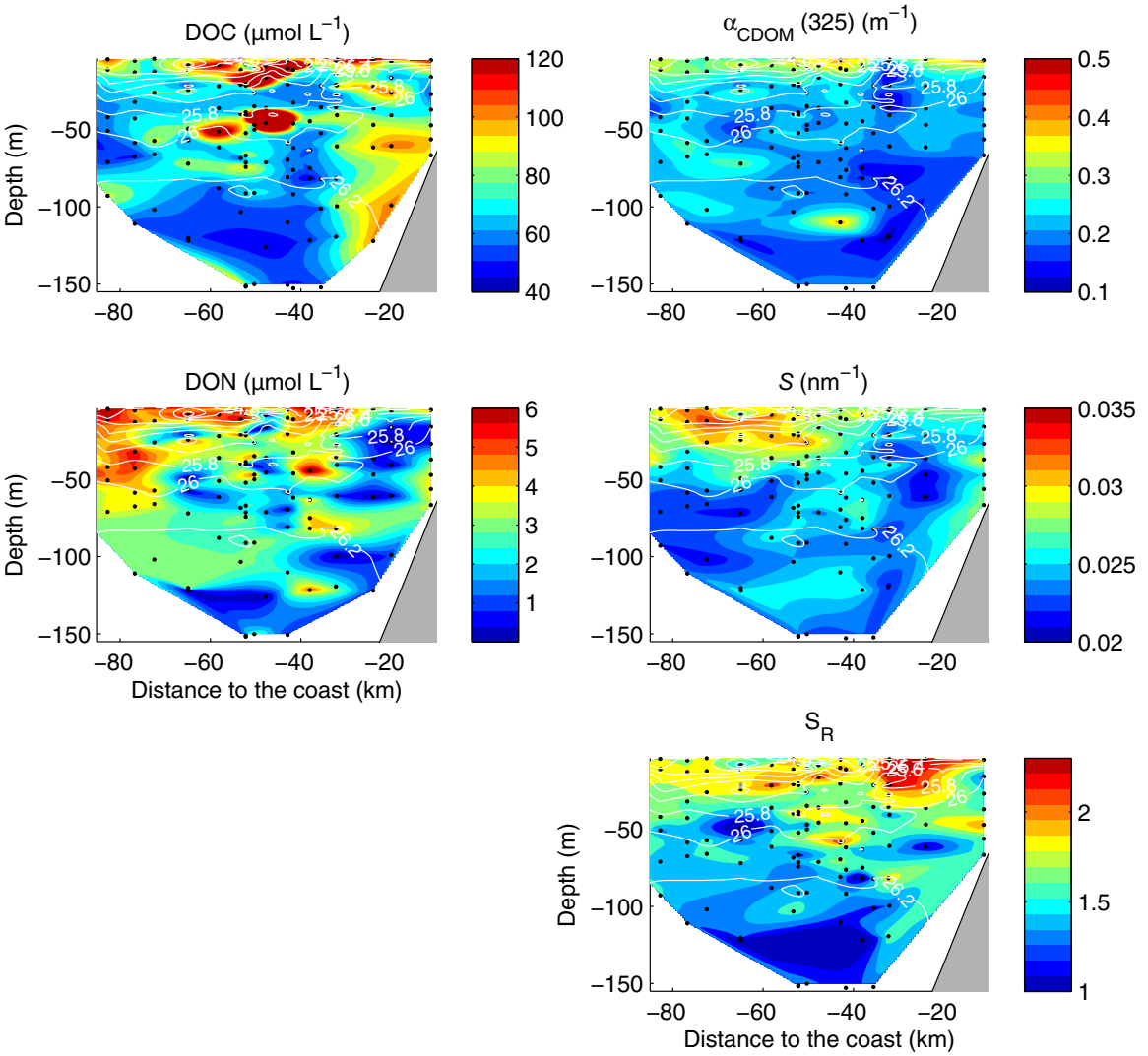

Figure 4. Vertical distributions of DOC, DON, CDOM at 325 nm (a_{CDOM} (325)), spectral slope ($S_{275-295}$) and spectral slope ratio (S_R) along the combined transect. The coastal slope is shaded in gray. Black dots represent the locations of taken samples. White isolines represent potential density distribution.

Little information is available on optically active DOM in the area off Peru. In the open Pacific, CDOM absorption at 325 nm ($a_{CDOM}(325)$) was previously reported to vary from 0.005 to 0.25 m^{-1} [*Swan et al*., 2009, *Nelson and Siegel*, 2013] and was reported to be controlled by microbial respiration, due to its significant covariance to apparent oxygen utilization in deep waters, and its accumulation with depth [*Swan et al*., 2009, *Nelson and Siegel*, 2013]. However, in our study, $a_{CDOM}(325)$ was highest in the upper 5–20 m of the water column with maximal values of ~0.5 m^{-1} in SSMW. CDOM absorption decreased at STSW, LNW and HNW up to 0.1 - 0.2 m^{-1} (Figure 4). This range of absorption values corresponds well to data reported for the surface microlayer by *Galgani and Engel* [2015] 2 months earlier at same area. In their study, $a_{CDOM}(325)$ varied from ~0.22 to 0.5 m^{-1} with a few very high values (0.75–1.25 m^{-1}) at the most nearshore stations.

CDOM spectral slope of 0.032 nm^{-1} was previously reported for the wavelength interval of 320–400 nm for South Pacific subtropical waters [*Nelson and Siegel*, 2013]. Off Peru, in the surface microlayer and upper 30 cm of the water column, $S_{275-295}$ ranged between 0.015 and 0.040 nm^{-1} [*Galgani and Engel*, 2015]. The distribution of $S_{275-295}$, in our study, revealed low values in HNW (<0.025 nm^{-1}) and higher values (>0.025 nm^{-1}) in SSMW and LNW (Figure 4 and supporting information Figure S1). Offshore, $S_{275-295}$ revealed a plume-like structure near the surface with highest values centered at 20 m depth, resembling the salinity plume associated with STSW.

S_R was also higher in STSW (~1.8) in comparison to HNW, where S_R ranged from 0.8 to 1.5. Its maximum values (>2), however, were found in SSMW and LNW (supporting information Figure S1 and Figure 4.). Previously, S_R was not reported for the water column off coast of Peru. It is known, however, that in open ocean waters S_R can vary from 1.5 to 4 [*Kowalczuk et al*., 2013, *Stedmon and Nelson*, 2015], while in terrestrially originated DOM S_R reached values <1 [*Stedmon and Nelson*, 2015]. For the surface microlayer and first 30 cm of water column S_R ranged from 0.7 to 5 [*Galgani and Engel*, 2015]. Hence, S_R results obtained in this study are in correspondence to previously published values and represent typical signatures of in situ produced marine DOM.

FDOM components were characterized by fluorescence at following Ex/Em wavelengths (in nm): component 1 (C1) – Ex/Em: 315/396–398, component 2 (C2) – Ex/Em: 355–365/420–480, component 3 (C3) – Ex/Em: 275/314–322, component 4 (C4) – Ex/Em: 290/352 and component 5 (C5) – Ex/Em: 405/490 (Figure 5).

Previous studies assigned Ex/Em characteristics similar to C1 (315/396–398) to humic-like substances produced in marine environment through microbial or, more generally, biological reworking of labile DOM ("peak M" in *Coble* [1996]; "peak β" in *Parlanti et al*. [2000]). Similar, in terms of spectral properties, to C1 fluorescent components were previously reported for the global ocean ("C4" in *Jørgensen et al*. [2011], "C2" in *Catalá et al*. [2016]). Those components were reported to vary from 0.001 to 0.025 RU in the upper 200 m of the water column, increasing with depth. Our findings are in agreement with previously reported values, as, during our study, C1 varied from 0.002 to 0.012 RU, and it was strongly depleted near the surface. Its highest fluorescence intensities, however, were mainly located at 10–100 m and did not correspond to any of defined waters (STSW, SSMW, LNW or HNW) (Figure 6).

Ex/Em characteristics (355–365/420–480) determined for C2, have been previously assigned to another humic-like component, i.e., "peak C" [*Coble*, 1996] or "α" [*Parlanti et al*., 2000] and have been referred to humic acids of terrestrial origin [*Parlanti et al*., 2000]. However, fluorescence signals similar to C2 were also found previously in the open ocean ("C1" in *Jørgensen et al*. [2011]; "C1" in *Catalá et al*. [2016]), with values increasing toward 200 m depth, ranging from 0.001 to 0.025 RU. In our study, C2 fluorescence intensities

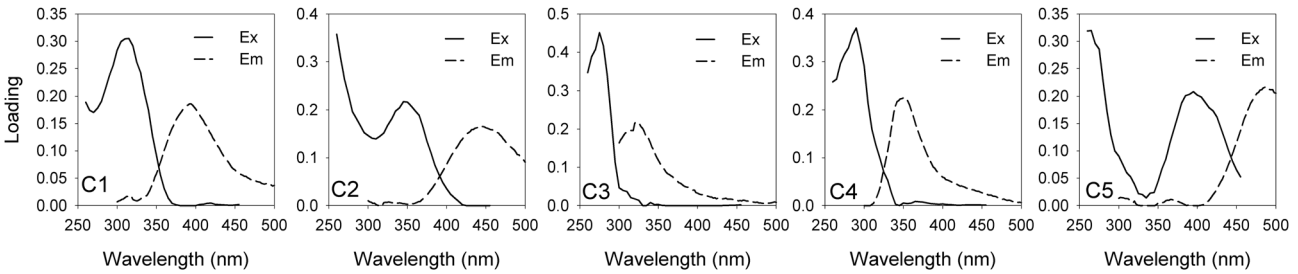

Figure 5. Spectral loadings (Ex/Em) of components C1–C5, identified during PARAFAC analysis.

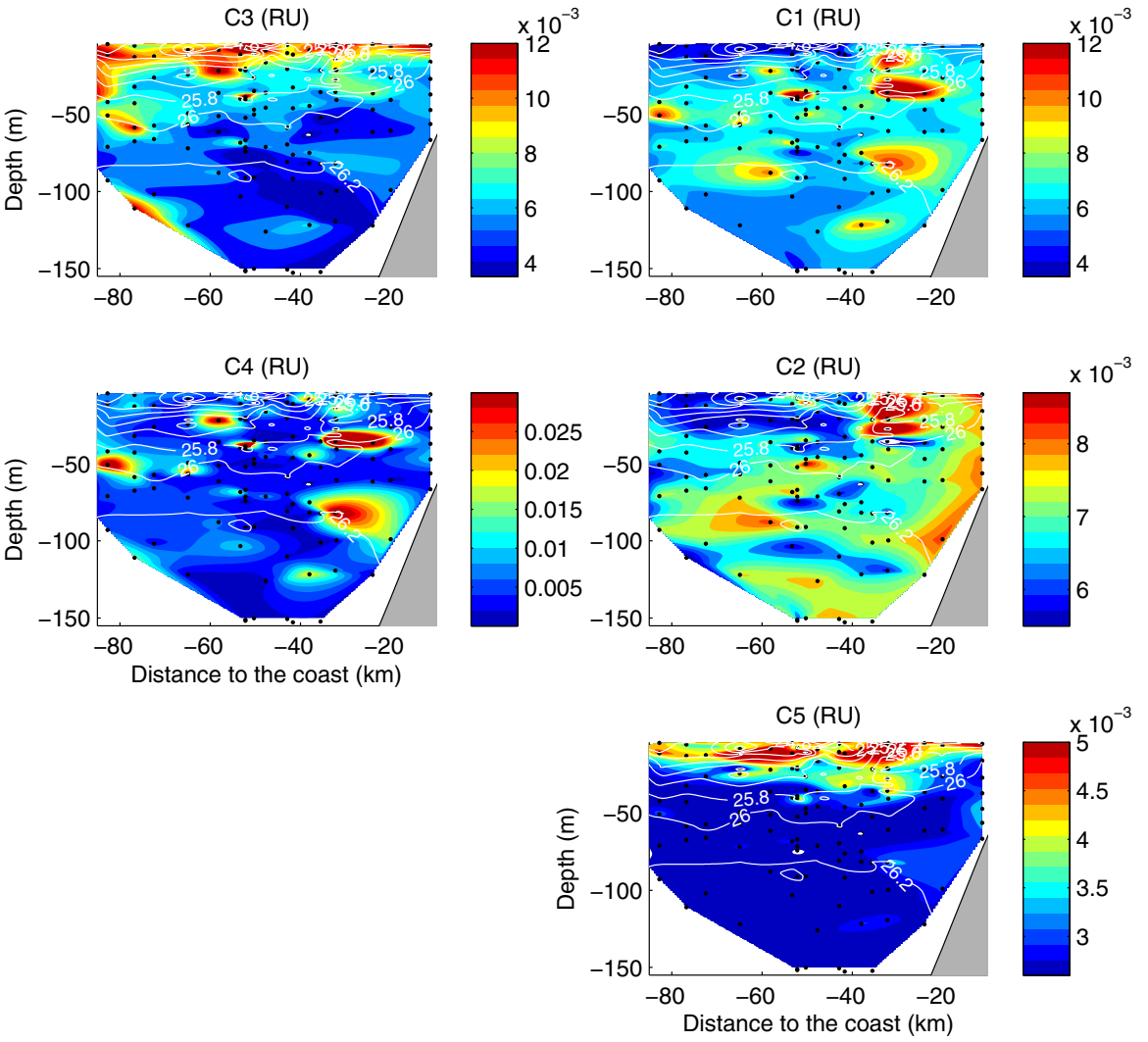

Figure 6. Vertical distributions of fluorescent components (C1–C5) along the combined transect. The coastal slope is shaded in gray. Black dots represent the locations of taken samples. White isolines represent potential density distribution.

varied between 0.005 and 0.010 RU. C2 was depleted within the upper 60 m at offshore stations. Highest C2 fluorescence intensities were determined near the sediments (LNW) and in the upper water column nearshore (SSMW). C2 intensities were also generally higher in HNW than at the surface STSW, but also yielded low values of 0.005–0.007 RU (Figure 6).

Ex/Em values of C3 (275/314–322) are characteristic for protein or amino acid-like substances ("peak B" in *Coble* [1996] or "γ" in *Parlanti et al.* [2000]). This component was referred to fresh, labile DOM that is produced at the exponential phase of phytoplankton growth [e.g., *Guéguen and Kowalczuk*, 2013] and during denaturation of proteins [*Determann et al.*, 1998]. Ex/Em characteristics similar to C3 were previously reported to be highest near the surface [*Jørgensen et al.*, 2011; *Catalá et al.*, 2016]. In our study, highest intensities of C3 were found in the upper euphotic zone (SSMW) (up to 0.02 RU), while at STSW, LNW and HNW they were less than 0.005 RU (Figure 6). C3 positively correlated to chl *a* (log(C3) versus log (chl *a*): $r^2=0.40$, $p<0.001$, n=133). Therefore, we refer to C3 as to phytoplankton-derived labile DOM during our study.

The distribution of C4 fluorescence was highly patchy, it ranged from 0.001 to >0.025 RU (Figure 6). Unlike C3, high values of C4 were observed near the surface as well as at depth. In the open ocean, similar, in terms of spectral properties, to C4 components have also been reported to be highly variable (0.001–0.080 RU) in the upper 200 m of the water column [*Jørgensen et al.*, 2011; *Catalá et al.*, 2016]. A component with similar

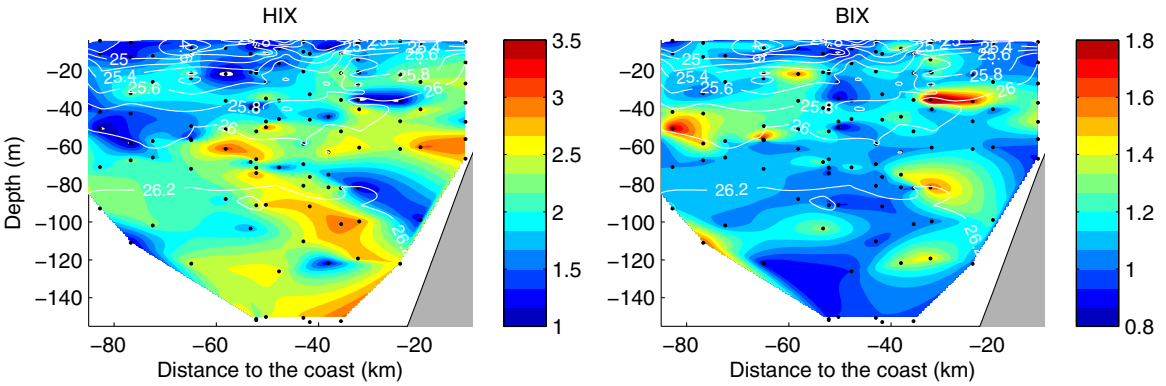

Figure 7. Vertical distributions of the biological index (BIX), calculated after *Huguet et al*. [2009] and of the humification index (HIX), calculated after *Zsolnay et al*. [1999]. The coastal slope is shaded in gray. Black dots represent the locations of taken samples. White isolines represent potential density distribution.

Ex/Em properties like C4, reported by *Catalá et al*. [2016], was highest at the deep chl *a* maximum. In our study, generally, higher C4 intensities (0.005 – 0.025 RU) could be associated to the depth of second ("deep") chl *a* maximum (50–80 m) as well, however, no strong correlation of C4 with chl *a* was determined (log(C4) versus log (chl *a*): $r^2=0.04$, $p<0.05$, n=133). Therefore, the interpretation of C4 cycling off the coast of Peru remains speculative.

The spectral characteristics of C5 signify its humic-like structure [*Kothawala et al*., 2013; *Yamashita et al*., 2008, 2013; *Guéguen et al*., 2014], as it reveals emission in visible wavelengths range. C5 intensities increased near the surface (up to 0.005 RU), indicating C5 production near the surface. Formation from biogenic precursors (see section 3.3), a red shift in the fluorescence of humic-like material after contact with sunlight, or a terrestrial input [*Murphy et al*., 2008] may have been potentially responsible for an accumulation of C5. *Stedmon and Markager* [2005] reported a new component, whose "fingerprint" was similar to Ex/Em of C5. They observed that in seawater exposed to light the fluorescence intensities of this component increased in presence of heterotrophic bacteria ("C7" in *Stedmon and Markager* [2005]). The component intensities decreased at same light conditions, when bacterial cells were filtered out ("C7" in *Stedmon and Markager* [2005]). In *Stedmon et al*. [2007], a humic-like component with similar spectral properties like C5 accumulated at the beginning of incubations of filtered Baltic Sea samples under light exposure. In the following stages of the incubations, the component was shown to be degraded. *Timko et al*. [2015] also reported of a C5-similar component, which was highly susceptible to light. As C2 and C5 occurred independently near the surface (Figure 6), and because the 5-component PARAFAC model was stable only for the upper water column, we speculate that formation and removal of C5 in the water column is induced by sunlight. However, the terrestrial origin of C5 may not be excluded, as humic-like fluorescence was previously mainly related to terrestrial sources [*Murphy et al*., 2008].

Biological/autochtonous index (BIX) values of 1–1.15 were measured between 40 and 60 m depth, while values <0.9 were observed in LNW (Figure 7). It has been suggested that an increase in BIX values indicate organic matter recently reworked by bacteria [*Parlanti et al*., 2000; *Huguet et al*., 2009; *Wilson and Xenopoulos*, 2009]. High BIX values in subsurface waters off coast of Peru therefore point to an intensive microbial reworking of DOM.

The humification index (HIX) increases as H/C ratio of the organic matter decrease, e.g., DOM is becoming "older" [*Zsolnay et al*., 1999]. During this study, highest HIX values of ~2–3 were measured at the vicinity to the sediment (LNW) and below the oxycline further offshore, pointing to high abundance of humified DOM. In contrast, HIX values were <1 in the upper 10–20 m, suggesting that optically active DOM there contained less humified or "younger" substances (Figure 7).

3.3. Processes Controlling the Distribution of Optically Active DOM

Based on the distribution of optically active DOM components and their properties during our study, we developed a conceptual model of DOM cycling in the ETSP off coast of Peru (Figure 8). The dimensions of the scheme correspond to those of the investigated transect (80 km offshore and 155 m deep). Locations of

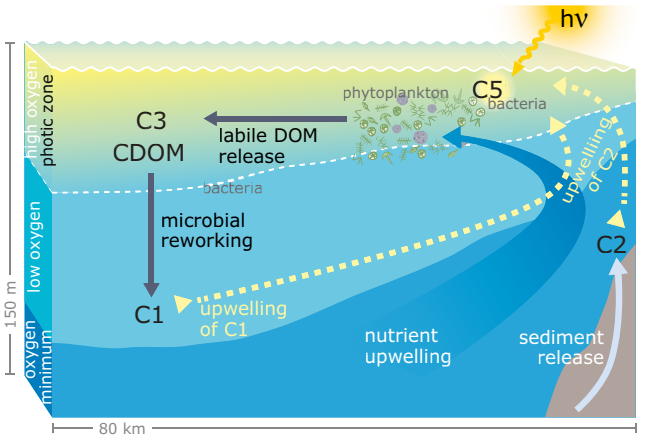

Figure 8. Schematic model of processes influencing the distribution of CDOM and FDOM in the investigated area off Peru. Symbols represent the prevailing components and arrows-dominating processes.

highest intensities/absorption coefficients of optically active DOM components are depicted. The arrows indicate processes, which most likely affect the distribution of the specified components.

Exposure to sunlight and upwelling of nutrients support high primary production and DOM release by phytoplankton, specifically during transition from nutrient replete to nutrient depleted conditions [*Goldman et al*., 1992; *Williams*, 1995; *Engel et al*., 2002; *Wetz and Wheeler*, 2003; *Conan et al*., 2007]. In accordance, accumulation of DOC in the upper 20 m of the water column indicated the production of fresh DOM components near the surface (Figure 3). The highest fluorescence intensities of the amino acid-like C3 mostly near the sea surface indicate that SSMW represents a water mass where DOM is freshly-produced (Figure 8). An increase of $a_{CDOM}(325)$ near the surface (0.2 to 0.5 m^{-1}) (Figure 3) suggested that phytoplankton is likely a direct source of CDOM in the area. This is in agreement to earlier studies showing e CDOM production by extracellular release of phytoplankton [*Romera-Castillo et al*., 2010] or by phytoplankton degradation or lysis [*Hu et al*., 2006; *Zhang et al*., 2009; *Organelli et al*., 2014].

In subsurface waters, highest fluorescence intensities of the marine humic-like C1 could be associated to microbial reworking of labile DOM (Figure 8), as components with spectral properties similar to C1 were previously shown to accumulate during microbial incubations (e.g., "C3" in *Stedmon and Markager* [2005]; *Lønborg et al*. [2010, 2015]; *Lønborg and Álvarez-Salgado* [2014]). The microbial in situ reworking in subsurface waters was also indicated by a presence of highest values of the biological index (BIX) (Figure 7).

Deeper in the water column, more refractory C2 revealed its high intensities (Figure 6). The refractory character of DOM at those depths is also indicated by increased values of HIX (Figure 7), which was previously shown to rise with DOM maturation [*Zsolnay et al*., 1999, *Zsolnay*, 2003]. Highest intensities of C2 fluorescence and HIX values were observed at the vicinity to inner shelf, where sediments were exposed to anoxia, and where an accumulation of DOC and DON was also recognized (Figure 4). Accumulation of DOC and DON in anoxic sediments primarily occurs via dissolution of particulate organic matter by biotic and abiotic processes [*Sierra et al*., 2001; *Deflandre et al*., 2002; *Burdige and Komada*, 2015]. Low molecular weight DOM obtained by those processes can be released to sediment pore waters [*Arnosti*, 2004; *Burdige and Komada*, 2015; *Chen and Hur*, 2015] and tend to form supramolecular associations via hydrogen or hydrophobic bonds [*Piccolo*, 2001] or polymers via reactions of condensation and complexation [e.g., *Finke et al*., 2007]. Both processes would lead to an increase in the apparent molecular weight of DOM and may explain higher HIX values observed near the sediment, as HIX values correlate directly with the apparent molecular weight of DOM [*Hur and Kim*, 2009]. The suggestion of sediment release is in correspondence to *Lomnitz et al*. [2015], who observed high inorganic P release from sediments a month earlier on same transect.

The humic-like, refractory C2 was found also near the surface in our study. We assume that upwelling was responsible for the transport of refractory DOM, such as C1 and C2, to the euphotic zone (Figure 8), where it undergoes reactions of photolysis [*Sulzberger and Durisch-Kaiser*, 2009]. Low fluorescence intensities of marine humic acids, represented by C1, near the surface could be explained by DOM photo-reactivity [*Kieber et al*., 1990; *Moran and Zepp*, 1997; *Sulzberger and Durisch-Kaiser*, 2009], as a component similar in terms of spectral properties to C1, was shown to be removed during photoreactions previously [*Chen et al*., 2010]. The presence of DOM modification by photoreactions in SSMW can also be supported by relatively high values of S_R (~2), as S_R was previously shown to increase, as CDOM is involved in photoreactions [*Helms et al*., 2008].

Intensive irradiation can activate protection mechanisms in microbial communities [*Kirchman*, 2012]. Heterotrophs may release various sunscreens to the water column, which protect microbial cell from damage; those substances include pigments and peroxidases among others [*Kirchman*, 2012]. As C5 accumulated solely within the sunlit surface ocean, it may represent a product of those photoreactions (Figure 8). Oxidative-polymerization of humic-like substances in the presence of peroxidase [*Jee et al*., 2010] or photochemical alteration of pigments [*Nelson*, 1993; *Cuny et al*., 1999] could be possible sources of C5 near the surface. As C5 was not enriched in STSW, we suggest that C5 undergoes further photo-degradation processes near the surface. This is in agreement with those studies, where components, similar to C5, in terms of spectral properties, were reported to be subject to photo-degradation [*Stedmon and Markager*, 2005*; Stedmon et al*., 2007; *Ishii and Boyer*, 2012; *Timko et al*., 2015].

3.4. Glider CDOM Measurements

The CDOM fluorescence measured by the WETStar fluorometer (WetLabs, USA) mounted onto the glider, resembled the distribution of C2. This can be explained by similar spectral EX/EM windows of the WETStar fluorometer (Ex/Em of 370/460 nm) and of C2 (Ex/Em: 355–365/420–480 nm). Highest fluorescence intensities were observed in the vicinity to sediments and lowest intensities were measured near the surface (Figure 9). Overall, a weak, but significant relationship was determined between WETStar CDOM measurements and C2 fluorescence intensities (r^2=0.32, p<0.001, n=45) (Figure 9).

Between 2 and 26 February, the glider measurements captured the development of a STSW plume, as indicated by high salinity (>35.25 g kg^{-1}) (Figure 10). The plume was associated with an onshore transport of very low WETStar CDOM fluorescence (<1.8 ppb), and is likely caused by horizontal eddy stirring [*Thomsen et al*., 2016].

The two intermediate water masses, ESSW and ESPIW that were shown to also influence the study area [*Thomsen et al*., 2016] revealed different WETStar CDOM fluorescence signatures. Low salinity ESPIW (<35.1 g kg^{-1}) showed slightly higher fluorescence intensities (~2.6 ppb) than ESSW (~2.3 ppb) characterized by medium salinity (~35.15 g kg^{-1}) (Figure 10).

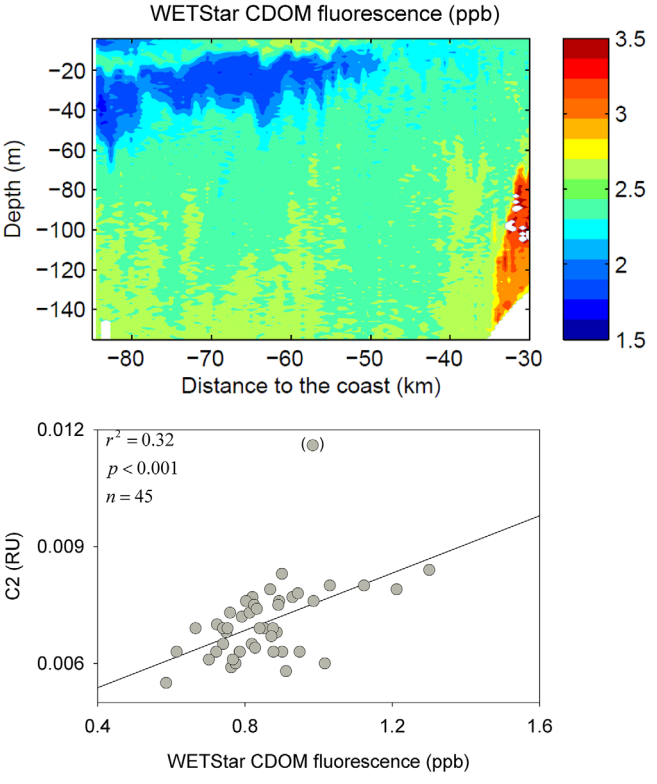

Figure 9. Distribution of CDOM fluorescence signal measured by the WETStar sensor, mounted on (top) a SLOCUM glider, and (bottom) its direct relationship to C2: The data point in brackets was considered as an outlier and was not included in the analysis.

Highest WETStar CDOM fluorescence was observed close to the seabed, suggesting a DOM release from the sediment (Figures 9 and 10). At the beginning of the M93 cruise (2–14 February), the WETStar CDOM fluorescence signal was transported to the surface and offshore (Figure 10). After 14–26 February, WETStar CDOM fluorescence near the surface was reduced (Figure 10). This may have been caused by the onshore advection of STSW diminishing the propagation of waters with high WETStar CDOM fluorescence to the surface and/or by lateral eddy stirring, which likely resulted in the offshore transport of the CDOM fluorescence signal [*Thomsen et al*., 2016]. Similar, in terms of spectral properties, to C2 components were previously shown to serve as ligands for trace metals ("peak A" in *Wu et al*. [2001]). WETStar CDOM fluorescence, which is measured at similar

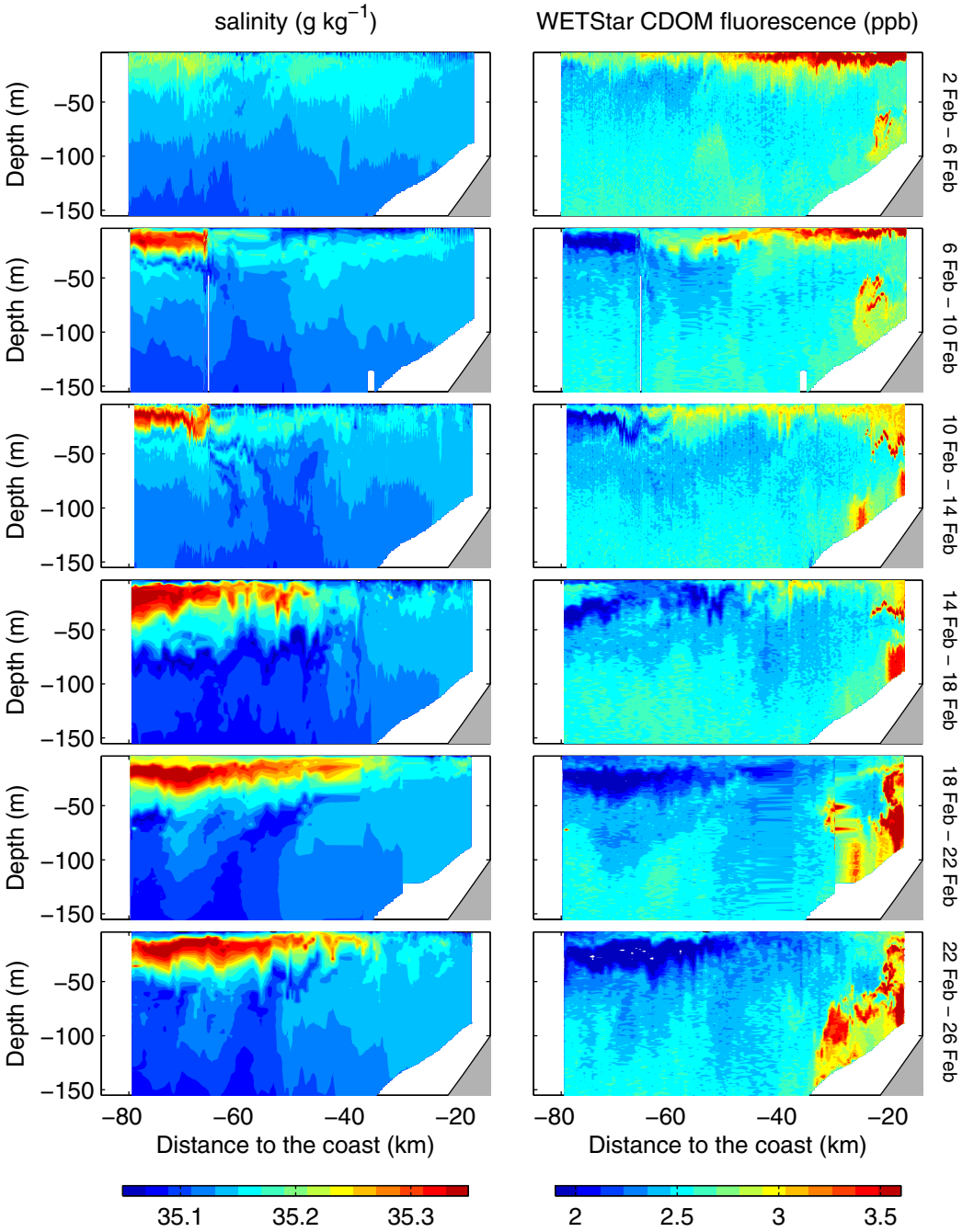

Figure 10. (left) Distribution of salinity as measured by the CTD sensor and (right) of CDOM fluorescence as measured by the WETStar sensor, mounted on a SLOCUM glider; from the right side the time periods, needed for the glider to complete the transect along its trajectory in one direction (nearshore-offshore/offshore-nearshore), are depicted. The coastal slope is marked as an area shaded in gray.

wavelengths to C2 "fingerprint," may, therefore, be helpful for tracing pathways of trace-metal transport in the ocean, e.g., linking sediment release and surface productivity.

During our study, the correlation of C2 with WETStar CDOM fluorescence was not very strong. This could be caused by particle scattering effects [*Saraceno et al.*, 2009; *Conmy et al.*, 2014], as higher turbidity (max 1.82 NTU) was measured at the most nearshore locations compared to stations offshore. Furthermore, the high variability of C2 fluorescence distribution in the water column, e.g., caused by the mesoscale eddy formation in the area [*Thomsen et al.*, 2016], is difficult to capture by discrete sampling. Moreover, glider

measurements and seawater sampling did not always occur at the same time at same location. Therefore, the correction to particle-scattering and water sampling of higher resolution, coupled to glider measurements, focusing on smaller spatial area would be needed for deriving a robust relationship between WET-Star CDOM fluorescence and C2.

4. Conclusions

In this study, the distribution of optically active DOM in and above the OMZ off Peru was described for the first time and we attempted to understand the underlying processes.

Our observations suggest that the ETSP off the coast of Peru represents a highly dynamic system in terms of DOM distribution and cycling, which is affected not only by biological processes (phytoplankton release, microbial reworking), but also by variable physical processes (eddy stirring, water mass transport, upwelling, sediment release, photoreactions). Optical properties of DOM, such as absorption and specific fluorescence (CDOM, C1–C5), can help to determine the different sources and modification processes of DOM and may also hint to its potential bioavailability in and above the OMZ.

Continuous CDOM fluorescence measurements with glider mounted sensors provided high spatial and temporal resolution measurements of humic-like DOM (C2) distribution and indicated a strong sediment-water column coupling on the shelf. Sampling for CDOM and FDOM from pore-water and the benthic boundary layer along with continuous glider-based measurements above the seabed may be a promising approach for developing quantitative estimates for DOM release from anoxic sediments. In this respect CDOM fluorescence, measured by glider mounted sensors, may be used as a tracer for studying benthic-pelagic coupling in OMZ regions.

Acknowledgments

This study was accomplished as a part of SFB754 project "Climate-Biogeochemical Interactions in the Tropical Ocean" of the Deutsche Forschungsgemeinschaft (dfg.de). The authors of this manuscript are not aware of any real or perceived financial conflicts of interests for other authors or authors that may be perceived as having a conflict of interest with respect to the results of this paper. We are very grateful to P. Kowalczuk and an anonymous reviewer for their valuable suggestions, which helped to improve the manuscript. We thank the chief scientists of M93 cruise G. Lavik and T. Kanzow for cruise planning and support during sampling, as well as the crew and scientists onboard RV METEOR during the M93 research cruise. We thank G. Lavik and G. Klockgether for nutrient data and are grateful to G. Krahmann for help in operating of the SLOCUM glider and for processing the CTD data, to R. Flerus and C. Mages for help with the water sampling, to J. Roa for the DOC/TDN analyses, to C. Karthäuser for help with the EEM sample-scanning, to L. Galgani for helpful discussions during writing of the manuscript and to R. Erven for support in graphic design. All data will be available at www.pangaea.de upon publication of the manuscript.

References

Arnosti, C. (2004), Speed bumps in the carbon cycle: Substrate structural effects on carbon cycling, *Mar. Chem.*, *92*, 263–273.

Azam, F., T. Fenchel, J. G. Field, J. S. Gray, L. A. Meyer-Reil, and F. Thingstad (1983), The ecological role of water-column microbes in the sea, *Mar. Ecol. Prog. Ser.*, *10*, 257–263.

Belzile, C., C. S. Roesler, J. P. Christensen, N. Shakhova, and I. Semiletov (2006), Fluorescence measured using the WETStar DOM fluorometer as a proxy for dissolved matter absorption, *Estuarine Coastal Shelf Sci.*, *67*, 441–449.

Biers, E. J., R. G. Zepp, and M. A. Moran (2007), The role of nitrogen in chromophoric and fluorescent dissolved organic matter formation, *Mar. Chem.*, *103*, 46–60.

Bricaud, A., A. Morel, and L. Prieur (1981), Absorption by dissolved organic matter of the sea (yellow substance) in the UV and visible domain, *Limnol. Oceanogr.*, *26*(1), 43–53.

Burdige, D. J., and T. Komada (2015), Sediment pore waters, in *Biogeochemistry of Marine Dissolved Organic Matter*, 2nd ed., edited by D. A. Hansell and C. A. Carlson, pp. 563–569, Elsevier, Oxford, U. K.

Catalá, T. S., et al. (2016), Drivers of fluorescent dissolved organic matter in the global epipelagic ocean, *Limnol. Oceanogr. Methods*, *61*(3), 1101–1119, doi:10.1002/lno.10281.

Chang B. X., J. R. Rich, A. Jayakumar, H. Naik, A. K. Pratihary, R. G. Keil,.B. B. Ward, and A. H. Devol (2014), The effect of organic carbon on fixed nitrogen loss in the eastern tropical South Pacific and Arabian Sea oxygen deficient zones, *Limnol. Oceanogr. Methods*, *59*(4), 1267–1274, doi:10.4319/lo.2014.59.4.1267.

Chen, M., and J. Hur (2015), Pre-treatments, characteristics, and biogeochemical dynamics of dissolved organic matter in sediments: A review, *Water Res.*, *79*, 10–25.

Chen, M., R. M. Price, Y. Yamashita, and R. Jaffé (2010), Comparative study of dissolved organic matter from groundwater and surface water in the Florida coastal Everglades using multi-dimensional spectrofluorometry combined with multivariate statistics, *Appl. Geochem.*, *25*, 872–880

Coble, P. G. (1996), Characterisation of marine and terrestrial DOM in seawater using excitation-emission matrix spectroscopy, *Mar. Chem.*, *51*, 325–346.

Coble, P. G (2007), Marine optical biogeochemistry: The chemistry of ocean color, *Chem. Rev.*, *107*(2), 402–418, doi:10.1021/cr050350+.

Conan, P., et al. (2007), Partitioning of organic production in marine plankton communities: The effects of inorganic nutrient ratios and community composition on new dissolved organic matter, *Limnol.Oceanogr. Methods*, *52*(2), 753–765.

Conmy, R. B., C. E. Del Castillo, B. D. Downing, and R. F. Chen (2014), Experimental design and quality assurance: In situ fluorescence instrumentation, in *Aquatic Organic Matter Fluorescence*, edited by P. G. Coble et al., pp. 190–230, Cambridge Univ. Press, N. Y.

Cuny, P., J.-C. Romano, B. Beker, and J.-F. Rontania (1999), Comparison of the photodegradation rates of chlorophyll chlorin ring and phytol side chain in phytodetritus: Is the phytyldiol versus phytol ratio (CPPI) a new biogeochemical index?, *J. Exp. Mar. Biol. Ecol.*, *237*(2), 271–290.

Deflandre, B., A. Mucci, J.-P. Gagné, C. Guignard, and B. J. Sunby (2002), Early diagenetic processes in coastal marine sediments disturbed by catastrophic sedimentation event, *Geochim. Cosmochim. Acta*, *66*(14), 2547–2558.

De Haan, H., and T. De Boer (1987), Applicability of light absorbance and fluorescence as measures of concentration and molecular size of dissolved organic carbon in humic Laken Tjeukemeer, *Water Res.*, *2*, 1731–734.

Del Castillo, C. E. (2007), Remote sensing of organic matter in coastal waters, in *Remote Sensing of Coastal Aquatic Environments: Technologies, Techniques and Applications*, edited by R. L. Miller, C. E. Del Castillo, and B. A. McKnee, pp. 157–180, Springer, Dordrecht, Netherlands.

Del Vecchio, R., and N. V. Blough (2004), On the origin of the optical properties of humic substances, *Environ. Sci.Technol.*, *38*(14), 3885–3891.
Determann, S., J. M. Lobbes, R. Reuter, and J. Rullköter (1998), Ultraviolet fluorescence excitation and emission spectroscopy of marine algae and bacteria, *Mar. Chem.*, *62*, 137–156.
Dickson, A. G., C. L. Sabine, and J. R. Christian (2007), Guide to best practices for ocean CO_2 measurements, *PICES Spec. Publ. 3, IOCCP Rep. 8*, 191 pp., North Pac. Mar. Sci. Organ., Sydney, Nova Scotia, Canada.
Echevin, V., O. Aumont, J. Ledesma, and G. Flores (2008), The seasonal cycle of surface chlorophyll in the Peru upwelling system: A modelling study, *Prog. Oceanogr.*, *79*, 167–176.
Engel, A., and L. Galgani (2015), The organic sea surface microlayer in the upwelling region off Peru and implications for air–sea exchange processes, *Biogeosci. Discuss.*, *12*, 10,579–10,619, doi:10.5194/bgd-12-10579-2015.
Engel, A., S. Goldthwait, U. Passow, and A. Alldredge (2002), Temporal decoupling of carbon and nitrogen dynamics in a mesocosm diatom bloom, *Limnol. Oceanogr.*, *47*(3), 753–761.
Engel A., C. Borchard, A. Loginova, J. Meyer, H. Hauss, and R. Kiko (2015), Effects of varied nitrate and phosphate supply on polysaccharidic and proteinaceous gel particle production during tropical phytoplankton bloom experiments, *Biogeosciences*, *12*, 5647–5665.
Fichot, C. G., and R. Benner (2012), The spectral slope coefficient of chromophoric dissolved organic matter ($S_{275\text{-}295}$) as a tracer of terrigenous dissolved organic carbon in river-influenced ocean margins, *Limnol. Oceanogr. Methods*, *57*(5), 1453–1466, doi:10.4319/lo.2012.57.5.1453.
Fiedler, P. C., and L. D. Talley (2006), Hydrography of the eastern tropical pacific: A review, *Prog. Oceanogr.*, *69*(2-4), 143–180, doi:10.1016/j.pocean.2006.03.008.
Finke, N., V. Vandieken, and B. B. Jørgensen (2007), Acetate, lactate, propionate, and isobutyrate as electron donors for iron and sulfate reduction in Arctic marine sediments, Svalbard, *FEMS Microbiol. Ecol.*, *59*, 10–22.
Franz, J. M. S., H. Hauss, U. Sommer, T. Dittmar, and U. Riebesell (2012), Production, partitioning and stoichiometry of organic matter under variable nutrient supply during mesocosm experiments in the tropical Pacific and Atlantic Ocean, *Biogeosciences*, *9*, 4629–4643, doi:10.5194/bg-9-4629-2012.
Galgani, L., and A. Engel (2015), Changes in optical characteristics of surface microlayers hint to photochemically and microbially-mediated DOM turnover in the upwelling region off Peru, *Biogeosci. Discuss.*, *12*, 19,373–19,421, doi:10.5194/bgd-12-19373-2015.
Goldman, J. C., D. A. Hansell, and M. R. Dennett (1992), Chemical characterization of three large oceanic diatoms: Potential impact on water column chemistry, *Mar. Ecol. Prog. Ser.*, *88*, 257–270.
Grasshoff, K., M. Ehrhardt, and K. Kremling (1983), *Methods of Seawater Analysis*, p. 419, Verlag Chemie, Weinheim, Germany.
Guéguen, C., and P. Kowalczuk (2013), Colored dissolved organic matter in frontal zones, in *Chemical Oceanography of Frontal Zones*, edited by I. M. Belkin, Springer, Berlin, doi:10.1007/698_2013_244.
Guéguen, C., C. W. Cuss, C. J. Cassels, and E. C. Carmack (2014), Absorption and fluorescence of dissolved organic matter in the waters of the Canadian Arctic Archipelago, Baffin Bay, and the Labrador Sea, *J. Geophys. Res. Oceans*, *119*, 2034–2047, doi:10.1002/2013JC009173.
Gunther, E. R. (1936), A report on oceanographic investigations in the Peru coastal current, *Discovery Rep.*, *13*, 107–276.
Harvey H. R., and S. A. Macko (1997), Kinetics of phytoplankton decay during simulated sedimentation: Changes in lipids under oxic and anoxic conditions, *Org. Geochem.*, *27*($^3/_4$), 129–140.
Helms, J. R., A. Stubbins, J. D. Ritchie, and E. C. Minor (2008), Absorption spectral slopes and slope ratios as indicators of molecular weight, source, and photobleaching of chromophoric dissolved organic matter, *Limnol. Oceanogr. Methods*, *53*(3), 955–969.
Hu, C., Z. Lee, F. E. Muller-Karger, K. L. Carder, and J. J. Walsh (2006), Ocean color reveals phase shift between marine plants and yellow substance, *IEEE Geosci. Remote Sens. Lett.*, *3*(2), 262–266.
Huguet, A., L. Vacher, S. Relexans, S. Saubussee, J. M. Froidefond, and E. Parlanti (2009), Properties of fluorescent dissolved organic matter in the Gironde Estuary, *Org. Geochem.*, *40*, 706–719, doi:10.1016/j.orggeochem.2009.03.002.
Hur, J., and G. Kim (2009), Comparison of the heterogeneity within bulk sediment humic substances from a stream and reservoir via selected operational descriptors, *Chemosphere*, *75*, 483–490.
Ishii, S. K. L., and T. H. Boyer (2012), Behavior of reoccurring PARAFAC components in fluorescent dissolved organic matter in natural and engineered systems: A critical review, *Environ. Sci. Technol.*, *46*, 2006–2017, doi:10.1021/es2043504.
Jayakumar, A., G. D. O'Mullan, S. W. A. Naqvi, and B. B. Ward (2009), Denitrifying bacterial community composition changes associated with stages of denitrification in oxygen minimum zones, *Microb. Ecol.*, *58*, 350–362, doi:10.1007/s00248-009-9487-y.
Jee, S. H., Y. J. Kim, and S. O. Ko (2010), Transformation of dissolved organic matter by oxidative polymerization with horseradish peroxidase, *Water Sci. Technol.*, *62*(2), 340–346, doi:10.2166/wst.2010.248.
Jetten, M. S., L. Niftrik, M. Strous, B. Kartal, J. T. Keltjens, and H. J. Op den Camp (2009), Biochemistry and molecular biology of anammox bacteria, *Crit. Rev. Biochem. Mol. Biol.*, *44*(2-3), 65–84, doi:10.1080/10409230902722783.
Jiao, N., et al. (2010), Microbial production of recalcitrant dissolved organic matter: Long-term carbon storage in the global ocean, *Nat. Rev. Microbiol.*, *8*, 593–599, doi:10.1038/nrmicro2386.
Jørgensen, L., C. A. Stedmon, T. Kragh, S. Markager, M. Middelboe, and M. Søndergaard (2011), Global trends in the fluorescence characteristics and distribution of marine dissolved organic matter, *Mar. Chem.*, *126*, 139–148, doi:10.1016/j,marchem.2011.05.002.
Kalvelage, T., G. Lavik, P. Lam, S. Contreras, L. Arteaga, C. R. Löscher, A. Oschlies, A. Paulmier, L. Stramma, and M. M. Kuypers (2013), Nitrogen cycling driven by organic matter export in the south pacific oxygen minimum zone, *Nat. Geosci.*, *6*(3), 228–234.
Kalvelage, T., et al. (2015), Aerobic microbial respiration in oceanic oxygen minimum zones, *PLoS One*, *10*(7), e0133526, doi:10.1371/journal.pone.0133526.
Kartal, B., M. M. Kuypers, G. Lavik, J. Schalk, H. J. Op den Camp, M. S. Jetten, M.Strous (2007), Anammox bacteria disguised as denitrifiers: Nitrate reduction to dinitrogen gas via nitrite and ammonium, *Environ. Microbiol.*, *9*, 635–642.
Keeling R. F., A. Körtzinger, and N. Gruber (2010), Ocean deoxygenation in a warming world, *Annu. Rev. Mar. Sci.*, *2*, 199–229.
Kieber, R. J., X. Zhou, and K. Mopper (1990), Formation of carbonyl compounds from UV-induced photodegradation of humic substances in natural waters: Fate of riverine carbon in the sea, *Limnol. Oceanogr.*, *35*, 1503–1515.
Kirchman, D. L. (2012), *Processes in Microbial Ecology*, 199 pp., Oxford Univ. Press, N. Y.
Kirchman, D. L., Y. Suzuki, C. Garside, and H. W. Duklow (1991), High turnover rates of dissolved organic carbon during a spring phytoplankton bloom, *Lett. Nat.*, *325*, 612–614.
Kothawala, D. N., C. A. Stedmon, R. A. Muller, G. A. Weyhenmeyer, S. J. Kohler, and L. J. Tranvik (2013), Controls of dissolved organic matter quality: Evidence from a large-scale boreal lake survey, *Global Change Biol.*, *20*, 1101–1114, doi:10.1111/gcb.12488.
Kowalczuk, P., M. Zabłocka, S. Sagan and L. Kuliński (2010), Fluorescence measured *in situ* as a proxy of CDOM absorption and DOC concentration in the Baltic Sea, *Oceanologia*, *52*(3), 431–471.

Kowalczuk, P., G. H. Tilstone, M. Zabłocka, R. Röttgers, and R. Thomas (2013), Composition of dissolved organic matter along and Atlantic Meridional Transect from fluorescence spectroscopy and Parallel Factor Analysis, *Mar. Chem.*, *157*, 170–184.
Kramer, G. D., and G. J. Herndl (2004), Photo- and bioreactivity of chromophoric dissolved organic matter produced by marine bacterioplankton, *Aquat. Microb. Ecol.*, *36*, 293–246.
Lee, C. (1992), Controls on organic carbon preservation: The use of stratified water bodies to compare intrinsic rates o decomposition in oxic and anoxic systems, *Geochim. Cosmochim. Acta*, *56*, 3323–3335.
Letscher, R. T., D. A. Hansell, C. A. Carlson, R. Lumpkin, and A. N. Knapp (2013), Dissolved organic nitrogen dynamics in global surface ocean: Distribution and fate, *Global Biogeochem. Cycles*, *27*, 141–153, doi:10.1029/2012GB004449.
Loginova, A. N., C. Borchard, J. Meyer, H. Hauss, R. Kiko, and A. Engel (2015), Effects of nitrate and phosphate supply on chromophoric and fluorescent dissolved organic matter in the Eastern Tropical North Atlantic: A mesocosm study, *Biogeosciences*, *12*, 6897–6914, doi: 10.5194/bg-12-6897-2015.
Lomnitz, U., S. Sommer, A. W. Dale, C. R. Löscher, A. Noffke, K. Wallmann, and C. Hensen (2015), Benthic phosphorus cycling in the Peruvian oxygen minimum zone, *Biogeosci. Discuss.*, *12*, 16,755–16,801.
Lønborg, C., and X. A. Álvarez-Salgado (2014), Tracing dissolved organic matter cycling in the eastern boundary of the temperate North Atlantic using absorption and fluorescence spectroscopy, *Deep Sea Res., Part I*, *85*, 35–46, doi:10.1016/j.dsr.2013.11.002.
Lønborg, C., X. A. Álvarez-Salgado, K. Davidson, S. Martínez-García, and E. Teira (2010), Assessing the microbial bioavailability and degradation rate constants of dissolved organic matter by fluorescence spectroscopy in the coastal upwelling system of the Ría de Vigo, *Mar. Chem.*, *119*(1-4), 121–129, doi:10.1016/j.marchem.2010.02.001.
Lønborg, C., T. Yokokawa, G. J. Herndl, and X. A. Álvarez-Salgado (2015), Production and degradation of fluorescent dissolved organic matter in surface waters of the eastern North Atlantic Ocean, *Deep Sea Res., Part I*, *96*, 28–37, doi:10.1016/j.dsr.2014.11.001.
Mopper, K., A. Stubbins, J. D. Ritchie, H. M. Bialk, and P. G. Hatcher (2007), Advanced instrumental approaches for characterization of marine dissolved organic matter: Extraction techniques, mass spectrometry, and nuclear magnetic resonance spectroscopy, *Chem. Rev.*, *107*, 419– 442, doi:10.1021/cr050359b.
Moran, M. A., and R. G. Zepp (1997), Role of photoreactions in the formation of biologically labile compounds from dissolved organic matter, *Limnol. Oceanogr.*, *42*, 1307–1316.
Murphy, K. R., C. A. Stedmon, T. D. Waite, and G. M. Ruiz (2008), Distinguishing between terrestrial and autochthonous organic matter sources in marine environments using fluorescence spectroscopy, *Mar. Chem.*, *108*(1–2), 40–58, doi:10.1016/j.marchem.2007.10.003.
Murphy, K. R., J. R. Boehme, C. Brown, M. Noble, G. Smith, D. Sparks and G. M. Ruiz (2013a), Exploring the limits of the dissolved organic matter fluorescence for determining seawater sources and ballast water exchange on the US Pacific coast, *J. Mar. Syst.*, *111-112*, 157–166.
Murphy, K. R., C. A. Stedmon, D. Graeber, and R. Bro (2013b), Fluorescence spectroscopy and multi-way techniques. PARAFAC, *Anal. Methods*, *5*, 6557–6566, doi:10.1039/c3ay41160e.
Nelson, J. R. (1993), Rates and possible mechanism of light-dependent degradation of pigments in detritus derived from phytoplankton, *J. Mar. Res.*, *51*, 155–179.
Nelson, N. B., and D. A. Siegel (2013), The global distribution and dynamics of chromophoric dissolved organic matter, *Annu. Rev. Mar. Sci.*, *5*, 447–476, doi:10.1146/annurev-marine-120710-100751.
Null, J. (2016), El Niño and La Niña years and intensities based on oceanic Niño Index, Golden Gate Weather Serv., Saratoga, Calif. [Available at www.ggweather.com/enso/oni.htm.]
Ogawa, H., Y. Amagai, I. Koike, K. Kaiser, and R. Benner (2001), Production of refractory dissolved organic matter by bacteria, *Science*, *292*, 917–920.
Organelli, E., A. Bricaud, D. Antoine, and A. Matsuoka (2014), Seasonal dynamics of light absorption by chromophoric dissolved organic matter (CDOM) in the NW Mediterranean Sea (BOUSSOLE site), *Deep Sea Res., Part I*, *91*(2014), 72–85, doi:10.1016/j.dsr.2014.05.003.
Parlanti, E., K. Wörz, L. Geoffroy, and M. Lamotte (2000), Dissolved organic matter fluorescence spectroscopy as a tool to estimate biological activity in a coastal zone submitted to anthropogenic inputs, *Org. Geochem.*, *31*, 1765–1781.
Pennington, J. T., K. L. Mahoney, V. S. Kuwahara, D. D. Kolber, R. Calienes, and F. P. Chavez (2006), Primary production in the eastern tropical pacific: A review, *Prog. Oceanogr.*, *69*(2-4), 285–317, doi:10.1016/j.pocean.2006.03.012.
Piccolo, A. (2001), The supramolecular structure of humic substances, *Soil Sci.*, *166*(11), 810–832.
Redfield, A. C. (1958), The biological control of chemical factors in the environment, *Am. Sci.*, *46*, 205–221.
Reid J. L., Jr. (1965), Intermediate waters of the Pacific Ocean, *Johns Hopkins Oceanogr. Stud.*, *2*, 85.
Revsbech, N. P. L. H. Larsen, J. Gundersen, T. Dalsgaard, O. Ulloa, and B. Thamdrup (2009), Determination of ultra-low oxygen concentrations in oxygen minimum zones by the stox sensor, *Limnol. Oceanogr. Methods*, *7*(5), 371–381, doi:10.4319/lom.2009.7.371.
Rochelle-Newall, E. J., F. D. Hulot, J. L. Janeau, and A. Merroune (2014), CDOM fluorescence as a proxy of DOC concentration in natural waters: A comparison of four contrasting tropical systems, *Environ. Monit. Assess.*, *186*, 589–596, doi:10.1007/s10661-013-3401-2.
Romankevich, E. A., and S. V. Ljutsarev (1990), Dissolved organic carbon in the ocean, *Mar. Chem.*, *30*, 161–178.
Romera-Castillo, C., H. Sarmento, X. A. Álvarez-Salgado, J. M. Gasol, and C. Marrase (2010), Production of chromophoric dissolved organic matter by marine phytoplankton, *Limnol. Oceanogr. Methods*, *55*(1), 446–454.
Saraceno, J. F., B. A. Pellerin, B. D. Downing, E. Boss, P. A. M. Bachand, and B. Bergamaschi (2009), A High Frequency in situ optical measurements during a storm event: Assessing relationships between dissolved organic matter, sediment concentration and hydrologic processes, *J. Geophys. Res.*, *114*, G00F09, doi:10.1029/2009JG000989.
Schneider, W., R. Fuenzalida, E. Rodriguez-Rubio, J. Garces-Vegas, and L. Bravo (2003), Characteristics and formation of eastern south pacific intermediate water, *Geophys. Res. Lett.*, *30*(11), 1581, doi:10.1029/2003GL017086.
Sierra, M. M. D., O. F. X. Donard, H. Etcheber, E. J. Soriano-Sierra, and M. Ewald (2001), Fluorescence and DOC contents of pore waters from coastal and deep-sea sediments in the Gulf of Biscay, *Org. Geochem.*, *32*, 1319–1328.
Silva, N., N. Rojas, and A. Fedele (2009), Water masses in the Humboldt Current System: Properties, distribution, and the nitrate deficit as a chemical water mass tracer for equatorial subsurface water off Chile, *Deep Sea Res., Part II*, *56*(16), 1004–1020, doi:10.1016/j.dsr2.2008.12.013
Spencer, R. G. M., L. Bolton, and A. Baker (2007), Freeze/thaw and pH effects on freshwater dissolved organic matter fluorescence and absorbance properties from a number if UK locations, *Water Res.*, *41*, 2941–2950.
Stedmon, C., and X. A. Álvarez-Salgado (2011), Shedding Light on a Black Box: UV-visible spectroscopic characterization of marine dissolved organic matter, in *Microbial Carbon Pump*, edited by N. Jiao, F. Azam, and S. Senders, pp. 62–63, Science/AAAS, Washington, D. C.
Stedmon, C. A., and R. Bro (2008), Characterizing dissolved organic matter fluorescence with parallel factor analysis: A tutorial, *Limnol. Oceanogr. Methods*, *6*, 572–579, doi:10.4319/lom.2008.6.572.

Stedmon, C. A., and S. Markager (2001), The optics of chromophoric dissolved organic matter (CDOM) in the Greenland Sea: An algorithm for differentiation between marine and terrestrially derived organic matter, *Limnol. Oceanogr.*, *46*(8), 2087–2093.
Stedmon, C. A., and S. Markager (2005), Tracing the production and degradation of autochtonous fractions of dissolved organic matter by fluorescence analysis, *Limnol. Oceanogr. Methods*, *50*(5), 1415–1426.
Stedmon, C. A., and N. Nelson (2015), The optical properties of DOM in the ocean, in *Biogeochemistry of Marine Dissolved Organic Matter*, 2nd ed., edited by D. A. Hansell and C. A. Carlson, pp. 481–508, Elsevier, Oxford, U. K.
Stedmon C. A., S. Markager, L. Tranvik, L. Kronberg, T. Slätis, and W. Martinsen (2007), Photochemical production of ammonium and transformation of dissolved organic matter in the Baltic Sea, *Mar. Chem.*, *104*, 227–240, doi:10.1016/j.marchem.2006.11.005.
Stramma, L., S. Hüttl, and J. Schafstall (2005), Water masses and currents in the upper tropical Northeast Atlantic off northwest Africa, *J. Geophys. Res.*, *110*, C12006, doi:10.1029/2005JC002939.
Strous, M., et al. (2006), Deciphering the evolution and metabolism of an anammox bacterium from a community genome, *Nature*, *440*, 790–794, doi:10.1038/nature04647.
Strub, P. T., J. M. Masias, V. Montecino, J. Rutllant, and S. Salinas (1998), Coastal ocean circulation off western South America, in *The Sea: The global Coastal Ocean 11*, 11th ed., edited by A. Robinson, and K. Brink, pp. 273–313, John Wiley, N. Y.
Sugimura, Y., and Y. Suzuki (1988), A high-temperature catalytic oxidation method for the determination of non-volatile dissolved organic carbon in seawater by direct injection of a liquid sample, *Mar. Chem.*, *24*, 105–131.
Sulzberger, B., and E. Durisch-Kaiser (2009), Chemical characterization of dissolved organic matter (DOM): A prerequisite for understanding UV-induced changes of DOM absorption properties and bioavailability, *Aquat. Sci.*, *71*, 104–126, doi:10.1007/s00027-008-8082-5.
Swan, C. M., D. A. Siegel, N. B. Nelson, C. A. Carlson, and E. Nasir (2009), Biogeochemical and hydrographic controls on chromophoric dissolved organic matter distribution in the Pacific Ocean, *Deep Sea Res., Part I*, *56*, 2172–2192.
Thieme, L., D. Graeber, M. Kaupenjohann, and J. Siemens (2016), Fast-freezing with liquid nitrogen preserves bulk dissolved organic matter concentrations, but not its composition, *Biogeosciences*, *13*, 4697–4705, doi:10.5194/bg-13-4697-2016.
Thomsen, S., T. Kanzow, G. Krahmann, R. J. Greatbatch, M. Dengler, and G. Lavik (2016), The formation of a subsurface anticyclonic eddy in the Peru-Chile Undercurrent and its impact on the near-coastal salinity, oxygen, and nutrient distributions, *J. Geophys. Res. Oceans*, *121*, 476–501, doi:10.1002/2015JC010878.
Timko, S. A., M. Gonsior, and W. J. Cooper (2015), Influence of oH on fluorescent dissolved organic matter photo-degradation, *Water Res.*, *85*, 266–274.
Wetz, M. S., and P. A. Wheeler (2003), Production and partitioning of organic matter during simulated phytoplankton blooms, *Limnol. Oceanogr.*, *48*, 1808–1817.
Williams, P. J. L. (1995), Evidence for the seasonal accumulation of carbon-rich dissolved organic material, its scale in comparison with changes in particulate material and the consequential effect on net C/N assimilation ratios, *Mar. Chem.*, *51*, 17–29.
Wilson, H. F., and M. A. Xenopoulos (2009), Effects of agricultural land use on the composition of fluvial dissolved organic matter, *Nat. Geosci.*, *2*(1), 37–41.
Winkler, L. W. (1888), Die Bestimmung des Wasser gelösten Sauerstoffes, *Ber. Dtsch. Chem. Ges.*, *21*(2), 2843–2854, doi:10.1002/cber.188802102122
Wood, A. M., and L. M. Van Valen (1990), Paradox lost? On the release of energy-rich compounds by phytoplankton, *Mar. Microb. Food Webs*, *4*, 103–116.
Wu, F., T. Midorikawa, and E. Tanoue (2001), Fluorescence properties of organic ligands for copper(II) in Lake Biwa and its rivers, *Geochem. J.*, *35*, 333–346.
Wyatt, K. H., R. J. Stevenson, and M. R. Turetsky (2010), The importance of nutrient co-limitation in regulating algal community composition, productivity, and algal-derived DOC in an oligotrophic marsh in interior Alaska, *Freshwater Biol.*, *55*, 1845–1860.
Wyrtki, K. (1967), Circulation and water masses in the eastern equatorial Pacific Ocean, *J. Oceanol. Limnol.*, *1*, 117–147.
Yamashita Y., R. M. Cory, J. Nishioka, K. Kuma, E. Tanoue, and R. Jaffe (2010), Fluorescence characteristics of dissolved organic matter in the deep waters of Okhotsk Sea and northwestern North Pacific Ocean, *Deep Sea Res., Part II*, *57*, 1478–1485.
Yamashita, Y., J. N., Boyer, and R. Jaffe (2013), Evaluating the distribution of terrestrial dissolved organic matter in a complex coastal ecosystem using fluorescence spectroscopy, *Cont. Shelf Res.*, *66*, 136–144.
Yamashita, Y., R. Jaffe, N. Maie, and E. Tanoue (2008), Assessing the dynamics of dissolved organic matter (DOM) in coastal environments by excitation emission matrix fluorescence and parallel-factor analysis (EEM-PARAFAC), *Limnol. Oceanogr. Methods*, *53*(5), 1900–1908.
Zhang, Y., M. A. van Dijk, M. Liu, G. Zhu, and B. Qin (2009), The Contribution of phytoplankton degradation to chromophoric dissolved organic matter (CDOM) in eutrophic shallow lakes: Field and experimental evidence, *Water Res.*, *43*, 4685–4697, doi:10.1016/j.waters.2009.07.024.
Zsolnay, A. (2003), Dissolved organic matter: Artefacts, definitions and functionds, *Geoderma*, *113*, 187–209, doi:10.1016/S0016-7061(02)00361-0.
Zsolnay, A., E. Baiger, E. Jimenez, B. Steinweg, and F. Saccomandi (1999), Differentiating with fluorescence spectroscopy the source of dissolved organic matter in soils subjected to drying, *Chemosphere*, *38*, 45–50, doi:10.1016/S0045-6535(98)00166-0.